2023 IEEE/ASME International Conference on Advanced Intelligent Mechatronics (AIM)
June 28-30, 2023. Seattle, Washington, USA

Convolutional Neural Network Based Denoising for Digital Image Correlation Reconstructing High-Fidelity Deformation Field

Bangyan Niu, and Jingjing Ji*, *Member, IEEE*

***Abstract*—Digital image correlation (DIC) is a widely used technique for full-field deformation measurement based on image processing. The high quality of images input for correlation is the most important guarantee for obtaining accurate physical field. In this paper, we propose a new method to deal with the negative effects of noise especially for deep learning-based DIC. Denoising convolutional neural network (DnCNN) block is introduced to deal with the noise before speckle patterns are fed into deep learning-based DIC. A new speckle pattern dataset, SPDataset, is created to train DnCNN on speckle features rather than on images with semantic information. The performance of networks trained on specific and blind noise level is compared and the possibility of network structure simplification is explored. The depth and performance of the network reach a good compromise at a layer number of 9. The denoising ability of the network for speckle patterns was confirmed qualitatively and quantitatively.**

I. Introduction

Digital image correlation (DIC) [1], as a full-field deformation measurement technique based on computer vision and image processing, has been widely applied in various advanced fields requiring experimental mechanics tasks, including damage/flaw evolution tracking [2], health monitoring [3], and mechanical response analysis [4]. By analyzing the pixel-level correlation between successive images, DIC algorithms enable the extraction of critical information such as strain distribution, surface deformation, and motion trajectories. During the measurement, images are taken before and after deformation, and distributed deformation field is determined by comparing intensity changes in the grayscale distribution of the image pair [5][6]. As illustrated with an experimental test in Fig.1, the displacement and strain fields are reconstructed using DIC based on speckle images correlation.

The high quality of images input for correlation is the most important guarantee for obtaining accurate physical field [7].

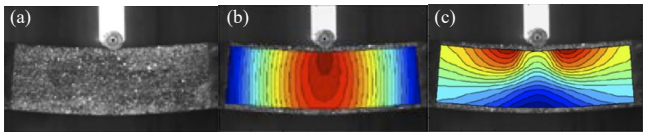

Figure 1. Illustration of DIC method [5]. (a) Speckle patterns captured for DIC calculation; (b)(c) colored cloud map representing the reconstructed deformation field based on underlying speckle images, where (b) for displacement field and (c) for strain field.

This work was supported in part by the National Key Research and Development Program of China under Grant 2019YFB1311005; in part by the National Science Foundation of China under Grant 52175510, Grant 52188102; and in part by Guangdong HUST Industrial Technology Research Institute, Guangdong Provincial Key Laboratory of Manufacturing Equipment Digitization under Grant 2020B1212060014.

B. Niu and J. Ji are with the State Key Lab. of Intel. Manuf. and Equip. Tech., Huazhong Univ. of Sci. and Tech., Wuhan, Hubei, 430074, P.R. China.

**Corresponding author: Jingjing Ji (email: jijingjing@hust.edu.cn)*

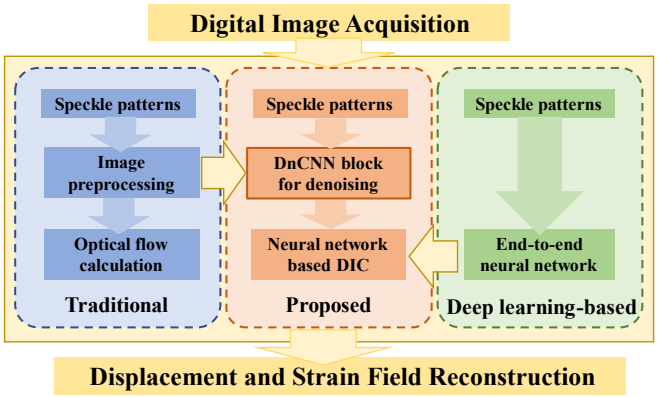

Figure 2. Illustration of the proposed preprocessing method.

However, due to factors such as camera shots and environmental influences, various defects are inevitably introduced in the process of digital image acquisition. Especially for the deformation analysis in motion, it is often necessary to acquire images in a moving environment, which makes it impossible to maintain consistent lighting and background and bring about a decrease in the quality of the acquired images. Therefore, extensive studies were conducted to obtain high-fidelity deformation fields by reducing the effect of image defects.

As illustrated in the flowchart of Fig. 2, a preprocessing step against contaminations between image acquisition and correlation is commonly incorporated in the traditional multi-step DIC. The effect of motion blur on the uncertainty of DIC measurements is investigated in [8] and a physical model is further developed. A zero-mean normalized sum of squared difference (ZNSSD) criterion is proposed by Pan *et al.* [9]. The normalization of the image grayscale values can effectively cope with the changes in ambient light during image acquisition. For the most common defect, noise, a Gaussian filter is commonly used for the generic approach. The effectiveness of the Gaussian low-pass filter for reducing the noise-induced error was verified experimentally in [7].

With the advancement of deep learning concepts and the increase of graphics processing unit (GPU) computing power, deep learning-based DICs are starting to emerge in recent years. Different from multi-step traditional DIC, end-to-end neural network is the remarkable feature of deep learning-based DICs. The traditional denoising method is no longer suitable to continue as preprocessing for deep learning-based DIC. That is because as a low-pass filter, Gaussian filtering will cause image smoothing, hindering the great advantage of neural networks being able to capture high-frequency deformation information.

For deep-learning based DIC, avoiding the negative effects of noise is mainly achieved by enabling the network to learn the mapping of noisy images to theoretical values. In

2021, Boukhtache *et al.* [10] constructed a new dataset, Speckle 2.0, by synthesized speckle pattern pairs. The images in Speckle 2.0 are all noisy to train the network to handle noise. By transfer learning and fine-tuning an optical flow estimation network, the StrainNets are established to estimate the displacement field. To incorporate as enriched deformation cases as possible in the dataset, Wang *et al.* [11] constructed the Hermite dataset with the help of the complex C^2 continuity Hermite element in the finite element method. The images in the Hermite dataset are with Gaussian noise level no more than 0.5% added. Yang *et al.* [12] further extended the quality variance of the images in the dataset. Defects such as sparse pattern, random large speckles, extra noises, and low contrast are included to increase the robustness and adaptivity of their proposed neural networks. In general, in the currently proposed deep learning-based DIC methods, noisy images are placed directly into the training set. However, a well-performing neural network to DIC is expected to cope with various quality of input images, the training set will become very large and the network architecture will be more complex. Meanwhile, the mathematical principle of image correlation indicates that theoretical deformation produces a direct mapping with noise-free images rather than noisy images. So as another widely studied challenge, image denoising is difficult to achieve expected results by relying on DIC neural networks alone, which is also confirmed by our experiments.

Inspired by image denoising before correlation in traditional multi-step DIC, in this paper, we propose a new preprocessing method to deal with the negative effects of noise especially for deep learning-based DIC. As shown in Fig. 2, the image denoising function is separated from the neural network used for DIC computation. Denoising convolutional neural network (DnCNN) [13] block is introduced to handle the noise of speckle patterns. We construct speckle pattern dataset, SPDataset, with specific and blind Gaussian noise level to train DnCNN. The possibility of a further lightweight network structure is also explored. The proposed method guarantees the image quality for the DIC input, allowing the subsequent DIC computation network to focus more on the relationship between the grayscale position change and the deformation field, thus improving the measurement performance.

The remainder of the paper is organized as follows.

(1) The network architecture for denoising is presented. The generation of speckle pattern dataset, SPDataset, and the training strategy for DnCNN are demonstrated.

2) The denoising performance of SPDataset-trained DnCNN is assessed qualitatively and quantitatively. The possibility of a further lightweight network structure is also explored.

3) The image pairs with and without SPDataset-trained DnCNN denoising are fed into a deep learning-based DIC method, StrainNet-h, and the results of displacement fields are reconstructed and compared.

II. Methodology

In this paper, a convolutional neural network-based denoising block (DnCNN) is used for image preprocessing of deep learning-based DIC method. The trained DnCNN denoising block will be performed before the speckle patterns are fed into the DIC network, thus ensuring the quality of input images. The DnCNN architecture is demonstrated together with the training dataset and training strategy in Section II. A new speckle pattern dataset, SPDataset, is constructed specifically to enable DnCNN to acquire the feature and the noise of speckle patterns.

A. DnCNN architecture

DnCNN [13] is introduced here for DIC denoising as the architecture is capable of remove Gaussian noise with unknown variance in the images. DnCNN is well-known for its good performance and has been adopted as a preprocessing fashion for many other optical measurement techniques, including digital holographic interferometry [14] and positron emission tomography [15].

The specific network structure is shown in Fig. 3. The input and output are the original speckle patterns f captured by the camera and the latent clean image g, respectively. The first layer contains convolution and rectified linear unit (ReLU). Since the speckle patterns are all single-channel grayscale images, convolution consist of 64 filter of size $3\times3\times1$. ReLU is an activation function, defined as (1).

$$\sigma(x) = \max(x, 0) \tag{1}$$

The last layer include only convolution with one filter of size $3 \times 3 \times 64$ to reconstruct the pattern from feature maps. Assume that the depth of DnCNN is D, layer 2~(D-1) are the same structure comprised of convolution (64 filters of size $3\times3\times64$), batch normalization and activation function $\sigma(x)$.

Residual learning [16] and batch normalization (BN) [17] are the two key characteristics of DnCNN. Residual learning avoids the problem of learning degradation and allows the depth of the network to be greatly extended. A single residual unit is adopted to obtain the residual image. Batch normalization is inserted between convolution and nonlinear activation. BN can mitigate the negative effects of variance shifts in each batch of data during training, such as training speed and network performance degradation.

The loss function $L(\omega)$ for speckle pattern denoising is defined as (2).

$$L(\omega) = \frac{1}{2N}\sum_{i=1}^{N}\|\sigma(f_i;\omega) - g_i\|_2^2 + \lambda\|\omega\|_2^2 \tag{2}$$

where f_i and g_i denoted the i^{th} noisy image and noise-free image, respectively. N is the number of image pairs in a mini batch. ω is the parameter that the neural network needs to learn. λ represents the weight decay coefficient of L_2 regularization, which contributes to avoid overfitting of the neural network.

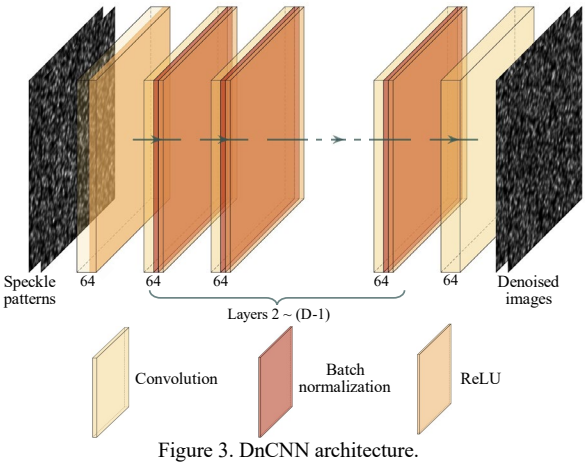

Figure 3. DnCNN architecture.

B. Speckle Pattern Dataset Generation

The original DnCNN is trained by the MatConvNet package. Unlike the package containing pictures of daily life scenes, the speckle pattern is composed of irregular scattered disks and have no semantic information. Therefore, we construct a new synthetic speckle pattern dataset, SPDataset, for the neural network training.

The images taken before and after deformation of the measured surface are denoted as reference image and current image, respectively. The relationship between the image pair is expressed as (3).

$$I_{cur}(x,y) = I_{ref}\left(x + D_x(x,y), y + D_y(x,y)\right) \quad (3)$$

where I_{ref} and I_{cur} denote the grayscale distribution of reference image and that of current image. D_x and D_y represent the displacement fields in the *x*- and *y*-directions.

As suggested in [18], the simulated speckle patterns are yielded by (4).

$$I_{ref}(\boldsymbol{s}) = \sum_{k=1}^{N} I_0 \exp\left(-\frac{|\boldsymbol{s} - \boldsymbol{i}_k|^2}{a^2}\right) \quad (4a)$$

$$I_{cur}(\boldsymbol{s}) = \sum_{k=1}^{N} I_0 \exp\left(-\frac{|\boldsymbol{s} - \boldsymbol{u}(\boldsymbol{s}) - \boldsymbol{i}_k|^2}{a^2}\right) \quad (4b)$$

where $\boldsymbol{s} = (x,y)$, and $\boldsymbol{i}_k$ is a random position within the pattern. The peak intensity I_0 =1, speckle size a=4, total number of speckles S=12000 and image size (800×800 pixels) are employed to generate image pairs.

It was pointed out that blindly expanding the size of the dataset brings only a small improvement in network performance [13]. Therefore, we constructed a large SPDataset and a small SPDataset with 400 images and only 5 images, respectively. The performance of the networks trained by different size datasets was compared in Section III.

C. Training Strategy

DnCNN has the ability to remove unknown levels of Gaussian noise. Ref.[13] employs two structures, DnCNN-S and DnCNN-B, with total layers of 17 and 20, respectively, to deal with specific and blind noise level. Since we will specifically discuss the effect of the network depth on the removal of speckle pattern noise in III.C, here a network with 20 layers is trained separately to deal with specific and blind noise level.

TABLE I. NETWORK NOMENCLATURE

DnCNN-αβ	Image noise	Dataset size
DnCNN-SS	specific $\sigma = 5$	small
DnCNN-SL	specific $\sigma = 5$	large
DnCNN-BS	blind $\sigma \in [1,9]$	small
DnCNN-BL	blind $\sigma \in [1,9]$	large

TABLE II. TRAINING PARAMETER

Parameter	Value
Max epoch	50
Mini batch size	128
Patch size	50×50
L2 regularization	1e-4
Momentum	0.9
Gradient threshold	0.005

Both the large and small SPDatasets are utilized to train the DnCNN with 20 layers. For clarity, the networks trained for different functions and by different size datasets are named as DnCNN-αβ, where $\alpha \in \{S, B\}$ denotes the network trained to handle specific or blind noise level, and $\beta \in \{S, L\}$ represents the network trained by small or large dataset.

For DnCNN- Sβ, the specific standard deviation of Gaussian white noise was set to $\sigma = 5$. Each image is randomly cropped into 256 patches and then randomly generated zero-mean Gaussian white noise with $\sigma = 5$, which means the noise is unique for each image patch.

For DnCNN-Bβ, the number of patches per image is set to 1280 to acquire more complex noise information. Noise with a standard deviation within the range $\sigma \in [1,9]$ is added to each patch.

Stochastic gradient descent (SGD) with momentum is utilized for training. The max epoch is 50, and the initial learning rate is set to 1e-1 and decays exponentially to 1e-4 within 50 epochs. Other training parameters are shown in Table II.

The training process of the networks is done in MATLAB (R2022a) and running on a personal computer (Intel Core i7-10875H 2.30GHz CPU, 16GB RAM, 64bit OS, NVIDIA TESLA V100 GPU). It takes 3 hours and 13 hours to train DnCNN-SL and DnCNN-BL, respectively.

III. RESULTS AND DISCUSSION

The denoising performance of SPDataset-trained DnCNN is demonstrated qualitatively and quantitatively. Firstly, single images are fed into DnCNN to evaluate the denoising ability of the network trained on SPDataset with different sizes and different noise levels. Further, the possibility of simplifying the DnCNN architecture is discussed based on denoising results. Finally, image pairs (image taken before and after deformation) with and without denoising are fed into a deep learning-based DIC for displacement field reconstruction, confirming the necessity and effectiveness of our proposed method.

A. Assessment of Denoising Results

1) Assessment of speckle patterns

A new speckle pattern is generated by (4a) and Gaussian noise with $\sigma = 5$ is then added to the pristine pattern. The noisy image is separately fed into pre-trained DnCNN (original DnCNN trained by the MatConvNet package) and SPDataset-trained DnCNN for comparison.

Fig. 4 presents the different states of the speckle pattern. Fig. 4(a) is the result after adding Gaussian white noise with $\sigma = 5$ to Fig. 4(d). It can be seen that the edges of speckles lose original smooth gradient variation and have obvious noise defects, which is more obvious in the magnified insets. After the denoising process of the pre-trained DnCNN, the noise is slightly moderated, but still significantly different from the pristine image. While the results after DnCNN-Sβ denoising are so much better that it is no longer possible to qualitatively describe their differences from the original images.

Fig. 5 quantitatively shows local structure similarity index measure (SSIM) [19] map of each image state. The darker the color, the lower the structural similarity between the current position and that in the pristine image. As in Fig. 5(b), the overall local SSIM maps are slightly lightened after the pre-

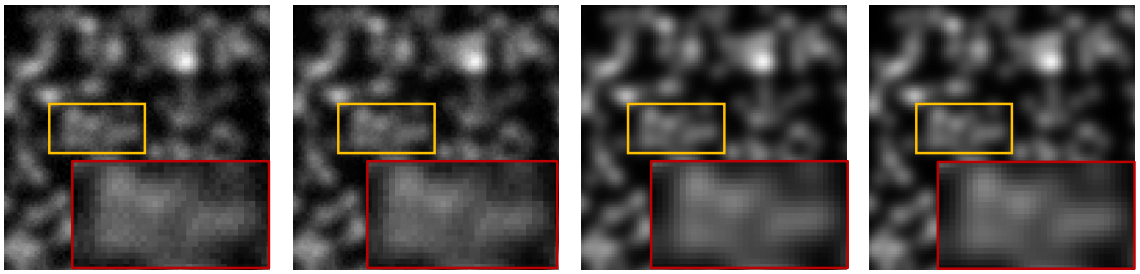

(a) Noisy (b) Pre-trained (c) DnCNN-SS (d) Noisefree

Figure 4. Speckle pattern and denoising results.
(a) Noisy $\sigma = 5$, (b) Denoised by pre-trained DnCNN, (c) Denoised by DnCNN-SS, (d) Noisefree.

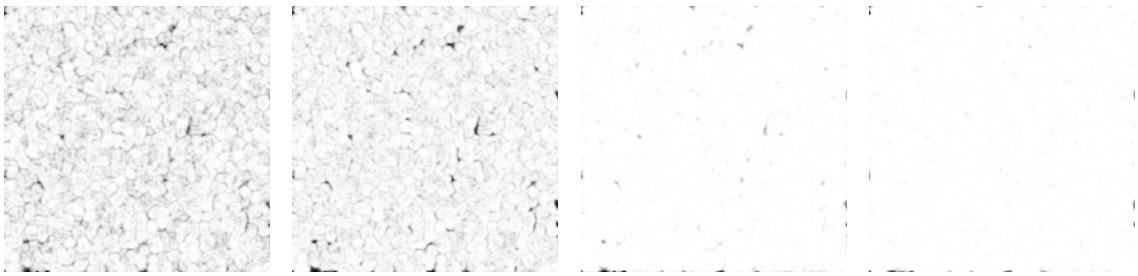

(a) Noisy Global SSIM: 0.9416 (b) Pre-trained Global SSIM: 0.9586 (c) DnCNN-SS Global SSIM: 0.9946 (d) DnCNN-SL Global SSIM: 0.9969

Figure 5. Comparison of local SSIM maps.
(a) Noisy $\sigma = 5$, (b) Denoised by pre-trained DnCNN, (c) Denoised by DnCNN-SS, (d) Denoised by DnCNN-SL.

trained DnCNN denoising. While shown in Fig. 5(c)(d), only individual dark points remain in the DnCNN trained on SPDataset. Especially the network trained on the larger dataset, the denoising results in only partial defects at the image boundaries.

Both Fig. 4 and Fig. 5 demonstrate that the SPDataset-trained network can correctly remove the noise from speckle patterns. Moreover, the SPDataset-trained DnCNN shows better denoising effect for speckle patterns than the pre-trained one, which indicates that DnCNN successfully learn from SPDataset to handle the features of speckle patterns that are different from images with semantic information.

2) Assessment of datasets performance

Datasets that are given different noise ranges and different sizes all have an impact on the final performance of the network training. Next, the performance of the networks trained by SPDataset under different conditions are compared.

For specific noise level and blind noise level, the training set is given a standard deviation (SD) of $\sigma = 5$ and $\sigma \in [1,9]$, respectively. The relationship between network names and datasets can be referred to Table I. Taking DnCNN-BL as an example, 'BL' denotes DnCNN being trained under 'Blind noise' and 'Large dataset' conditions.

To better reflect network performance, together with SSIM, the peak signal-to-noise ratio (PSNR) is also used to quantitatively measure the effect of image denoising. Larger PSNR value means better denoising effect.

Table. III lists the quantitative assessment of denoising performance under different training conditions, where the best metrics at the same noise level are marked in bold in each row. Some observations can be made from Table III:

1) All the bold appears in the larger dataset columns, which indicates the results from networks trained by large datasets show better performance than those trained by small ones.

2) Network trained with the specific noise level have effects in the vicinity of their noise levels beyond those based on blind noise training. This is because the uniformity of the sample makes it more focused on specific level of noise features. It is noteworthy that despite this difference, the margin between DnCNN-SL and DnCNN-BL on both SSIM and PSNR is only 1% and 0.05%, respectively.

3) However, blind denoising has much better processing performance when noise level moving away from that particular value, especially when the noise becomes larger. At the noise level of $\sigma = 9$, the performance of DnCNN-BS is already comparable to that of DnCNN-SL.

Besides, training on small dataset can be done in ten minutes, while large training sets take tens of times longer. Although the large SPDataset-based networks always outperform the ones training on the small SPDataset, the performance gap from dataset sizes is all within 3%. This indicates that the proposed DnCNN structure can perform well for speckle pattern denoising even after a short time and small dataset training.

B. Simplification of the DnCNN Architecture

In addition to the datasets, the depth of CNN architecture is also a major factor in performance. The above experiments all used a neural network structure with 20 hidden layers, which has the possibility of parameter redundancy. Here we explore the impact of simplifying the network structure on performance.

As shown in Fig. 3, layer 2 to layer (D-1) are the same structure consisting of convolution, batch normalization and ReLU. We set the total number of layers D from 3 to 17 in step of 2. Large SPDataset (400 speckle patterns) are used and each image is randomly cropped into 256 patches of 50×50 pixels.

TABLE III. QUANTITATIVE EVALUATION OF IMAGES

Noise level (SD)	Noisy		Denoised							
			DnCNN-SS		DnCNN-SL		DnCNN-BS		DnCNN-BL	
	PSNR	SSIM	PSNR	SSIM	PSNR	SSIM	PSNR	SSIM	PSNR	SSIM
1	47.8247	0.9970	51.3461	0.9988	51.9352	0.9990	52.0611	0.9990	**52.3274**	**0.9991**
2	42.0838	0.9892	49.7982	0.9983	**50.5178**	**0.9987**	50.1766	0.9984	50.3338	**0.9987**
3	38.6412	0.9767	47.9851	0.9973	**48.8550**	**0.9982**	48.2032	0.9973	48.4453	0.9981
4	36.1680	0.9604	46.3362	0.9961	**47.3790**	**0.9976**	46.5063	0.9960	46.9273	0.9974
5	34.2899	0.9413	44.7662	0.9943	**45.9173**	**0.9967**	44.9730	0.9941	45.5257	0.9965
6	32.7120	0.9193	43.3297	0.9921	**44.6054**	**0.9955**	43.6496	0.9921	44.3315	0.9954
7	31.4259	0.8961	42.0560	0.9895	**43.5009**	0.9941	42.6137	0.9901	43.3796	**0.9944**
8	30.2769	0.8709	40.9212	0.9852	42.1806	0.9916	41.4337	0.9874	**42.3362**	**0.9928**
9	29.2781	0.8449	39.0448	0.9800	40.8065	0.9886	40.3961	0.9846	**41.3654**	**0.9913**

SD: Standard Deviation

The max epoch number is set to 20. Other training parameters remain the same from those in III.A.

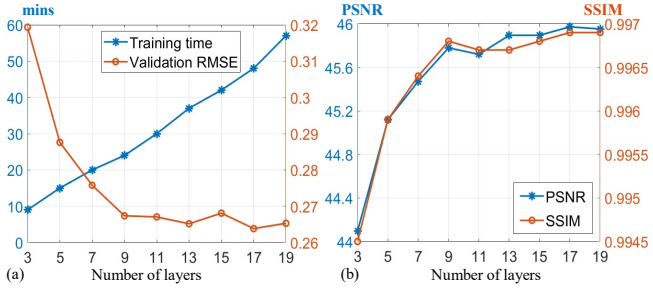

Figure 6. Performance of the network with different number of layers during (a) Training, (b) Denoising.

The performance of the network with different layers (including layer 20) for both training and application is presented in Fig. 6. Shown in Fig. 6 (a), as the number of network layers increases, the time required for training rises, while the error on the validation dataset decreases rapidly at the beginning and starts to level off and fluctuate after the number of layers reaches 9.

The denoising performance trend of the network with different layer numbers basically matches that of the validation RMSE. Both PSNR and SSIM increasing at the beginning, and similarly oscillating and slowly moving upward after the layer number reaches 9. Therefore, the network achieves a balance between depth and performance at a layer number of 9.

C. Illustration of displacement fields reconstruction

Further, the image pairs with and without denoising are fed into StrainNet-h [10] to obtain the displacement field. StrainNet-h is a fine-tuned architecture from optical flow neural network, which can perform the task of image correlation in conventional DIC. It is worth noting that the computational accuracy of this network itself is not within the scope of this paper.

Referring to Sample 14 in DIC Challenge [20], the *x*-direction displacement with a constant periodic sinusoidal variation (5) in size is employed as a theoretical value to generate the speckle image pair by (4). The theoretical displacement field is shown in Fig. 7(f).

$$u(x) = -2\sin\left[\frac{2\pi(x-20)}{180}\right] \tag{5}$$

The displacement field errors derived from StrainNet-h are evaluated in terms of root-mean-square error (RMSE).

$$\mathrm{RMSE} = \sqrt{\frac{1}{n}\sum_{i=1}^{n}(\boldsymbol{u}_i - \boldsymbol{u}_{ti})^2} \tag{6}$$

where n represents the number of pixels in the evaluation region. $\boldsymbol{u}_i$ and $\boldsymbol{u}_{ti}$ denote the experimental and theoretical values, respectively.

Fig. 7 illustrate *x*-directional displacement fields derived from StrainNet-h. Some findings can be made in the following:

1) By comparing Fig. 7(a) with Fig. 7(e), it can be seen that the computational accuracy of the noise-free image input to the network is much higher than that of the image with noise. This means that deep learning-based DICs have difficulty in avoiding noise defects when performing image correlation, which indicates that our proposed idea of adding a denoising module before the end-to-end neural network is imperative.

2) As shown in Fig. 7(b), the displacement field obtained after pre-trained DnCNN denoising have a 5.60% improvement in the accuracy. This improvement is mainly found at the crest and trough of the sine curve. While the accuracy of displacement fields derived from the images denoised by the SPDataset-trained networks have a much better performance than the pre-trained model, 35.65% and 36.98% for the small and large dataset, respectively. The result differences between images denoised by DnCNN-SS and DnCNN-SL (Fig. 7(c)(d)) and noisefree (Fig. 7(e)) are too slight to be visually noticed. The conclusion is consistent with the results of the comparison between the above speckle patterns, shown in Fig. 4 and Fig. 5.

IV. CONCLUSION

This paper proposes a new preprocessing method for deep learning-based DIC to separate the image denoising function from neural network-based correlation. The main contributions of this paper are summarized as follows:

1) Denoising convolutional neural network (DnCNN) block is introduced to deal with the noise before speckle patterns are fed into deep learning-based DIC. The denoising

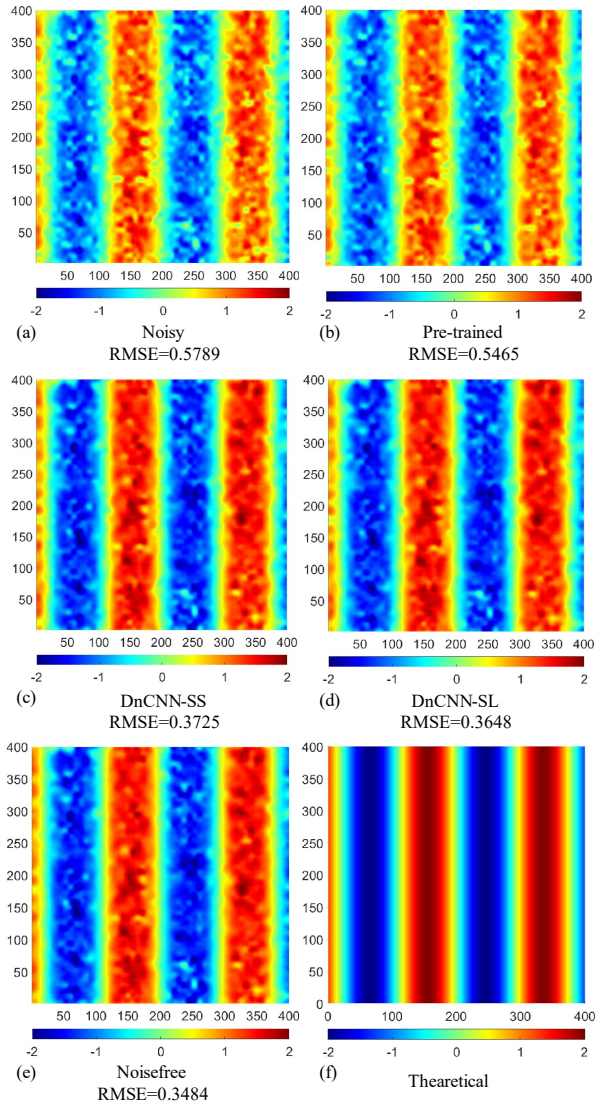

Figure 7. *X*-directional displacement fields obtained by StrainNet-h based on speckle patterns after different processing.

performance of the network is qualitatively and quantitatively proven to be effective.

2) A speckle pattern dataset, SPDataset, is constructed to enable the neural network to be trained on the speckle pattern features and noise. Experiments show that the displacement field derived after SPDataset-trained DnCNN denoising can achieve a 36.98% improvement in the accuracy, while only 5.60% for pre-trained DnCNN.

3) The performance of networks trained on SPDatasets of different sizes and different noise levels is compared. The simplification of the DnCNN architecture is explored. The depth and performance of the network reach a good compromise at a layer number of 9.

Enhancing the quality of image inputs for DIC holds significant implications for the mechatronics domain. The improved accuracy and reliability of DIC measurements enable engineers and researchers to gain deeper insights into the mechanical behavior of robotics systems, facilitating better design optimization, structural analysis, and performance evaluation. It is worth noting that while the preprocessing of deep learning-based DIC explored in this paper is mainly embodied in denoising, defects such as motion blur and ambient light changes are all worth trying in the preprocessing stage.

REFERENCES

[1] M. A. Sutton, J.-J. Orteu, and H. W. Schreider, *Image Correlation for Shape, Motion and Deformation Measurements: Basic Concepts, Theory and Applications.* USA, NY, USA: Springer, 2009.

[2] S. Zafar, A. Hedayat, and O. Moradian, "Evolution of tensile and shear cracking in crystalline rocks under compression," *Theor. Appl. Fract. Mec.,* vol. 118, Apr. 2022.

[3] Y. Huang, K. M. Lee, J. Ji, and W. Li, "Digital image correlation based on primary shear band model for reconstructing displacement, strain, and stress fields in orthogonal cutting," *IEEE-ASME Trans. Mech.*, vol. 25, no. 4, pp. 2088-2099, Aug. 2020.

[4] G. Sierra, B. Wattrisse, and C. Bordreuil, "Structural analysis of steel to aluminum welded overlap joint by digital image correlation," *Exp. Mech.,* vol. 48, no. 2, pp. 213-223, Apr. 2008.

[5] B. Pan, "Digital image correlation for surface deformation measurement: historical developments, recent advances and future goals," *Mea. Sci. Tech.*, vol. 29, no. 8, Aug. 2018.

[6] Y. Huang, J. Ji, and K. M. Lee, "Model-based digital image correlation for noncontact deformation measurement of strain field and mechanical property," *IEEE Trans. Indus. Inform.*, vol. 15, no. 9, pp. 5109-5118, Sep. 2019.

[7] B. Pan, "Bias error reduction of digital image correlation using Gaussian pre-filtering," *Opt. Laser Eng.,* vol. 51, no. 10, pp. 1161-1167, Oct. 2013.

[8] A. Lavatelli and E. Zappa, "A displacement uncertainty model for 2-D DIC measurement under motion blur conditions," *IEEE Trans. Instrum. Meas.,* vol. 66, no. 3, pp. 451-459, Mar. 2017.

[9] B. Pan, H. Xie, and Z. Wang, "Equivalence of digital image correlation criteria for pattern matching," *Appl. Opt.*, vol. 49, no. 28, pp. 5501–5509, 2010.

[10] S. Boukhtache, K. Abdelouahab, F. Berry, B. Blaysat, M. Grediac, and F. Sur, "When Deep Learning Meets Digital Image Correlation," *Opt. Laser Eng.,* vol. 136, Jan. 2021.

[11] Y. Wang and J. Q. Zhao, "DIC-Net: Upgrade the performance of traditional DIC with Hermite dataset and convolution neural network," *Opt. Laser Eng.,* Article vol. 160, p. 13, Jan. 2023.

[12] R. Yang, Y. Li, D. Zeng, and P. Guo, "Deep DIC: Deep learning-based digital image correlation for end-to-end displacement and strain measurement," *J. Mater. Process Tech.,* vol. 302, Apr. 2022.

[13] K. Zhang, W. M. Zuo, Y. J. Chen, D. Y. Meng, and L. Zhang, "Beyond a Gaussian Denoiser: Residual Learning of Deep CNN for Image Denoising," *IEEE Trans. Image Process,* vol. 26, no. 7, pp. 3142-3155, Jul. 2017.

[14] J. S. Shi, X. J. Zhu, H. Y. Wang, L. M. Song, and Q. H. Guo, "Label enhanced and patch based deep learning for phase retrieval from single frame fringe pattern in fringe projection 3D measurement," *Opt. Express,* vol. 27, no. 20, pp. 28929-28943, Sep. 30, 2019.

[15] K. Kim *et al.*, "Penalized PET Reconstruction Using Deep Learning Prior and Local Linear Fitting," *IEEE Trans. Medical Imaging,* vol. 37, no. 6, pp. 1478-1487, Jun. 2018.

[16] K. He, X. Zhang, S. Ren, and J. Sun, "Deep residual learning for image recognition," in Proc. *IEEE Conf. Comput. Vis. Pattern Recognit.*, Jun. 2016, pp. 770–778.

[17] S. Ioffe and C. Szegedy, "Batch normalization: Accelerating deep network training by reducing internal covariate shift," *Proc. Int. Conf. Mach. Learn.*, vol. 37, pp. 448-456, 2015.

[18] P. Zhou, "Subpixel displacement and deformation gradient measurement using digital image/speckle correlation (DISC)," *Opt. Eng.*, vol. 40, no. 8, 2001.

[19] Zhou, W., A. C. Bovik, H. R. Sheikh, and E. P. Simoncelli. "Image Quality Assessment: From Error Visibility to Structural Similarity." *IEEE Trans. Image Proc*. Vol. 13, Issue 4, pp. 600–612, Apr. 2004.

[20] P. L. Reu *et al.*, "DIC Challenge: Developing Images and Guidelines for Evaluating Accuracy and Resolution of 2D Analyses," *Exp. Mech.,* vol. 58, no. 7, pp. 1067-1099, Sep. 2018.